Submitted to the Annals of Applied Statistics

PHOTODEGRADATION MODELING BASED ON LABORATORY ACCELERATED TEST DATA AND PREDICTIONS UNDER OUTDOOR WEATHERING FOR POLYMERIC MATERIALS

By Yuanyuan Duan, Yili Hong, William Q. Meeker, Deborah L. Stanley, and Xiaohong Gu

Virginia Tech, Iowa State University, and National Institute of Standards & Technology

Photodegradation, driven primarily by ultraviolet (UV) radiation, is the primary cause of failure for organic paints and coatings, as well as many other products made from polymeric materials exposed to sunlight. Traditional methods of service life prediction involve the use of outdoor exposure in harsh UV environments (e.g., Florida and Arizona). Such tests, however, require too much time (generally many years) to do an evaluation. To overcome the shortcomings of traditional methods, scientists at the U.S. National Institute of Standards and Technology (NIST) conducted a multi-year research program to collect necessary data via scientifically-based laboratory accelerated tests. This paper presents the statistical modeling and analysis of the photodegradation data collected at NIST, and predictions of degradation for outdoor specimens that are subjected to weathering. The analysis involves identifying a physics/chemistry-motivated model that will adequately describe photodegradation paths. The model incorporates the effects of explanatory variables which are UV spectrum, UV intensity, temperature, and relative humidity. We use a nonlinear mixed-effects model to describe the sample paths. We extend the model to allow for dynamic covariates and compare predictions with specimens that were exposed in an outdoor environment where the explanatory variables are uncontrolled but recorded. We also discuss the findings from the analysis of the NIST data and some areas for future research.

1. Introduction.

1.1. *The Problem and NIST Experiments.* Polymeric materials are widely used in many products such as paints, coatings, and components in systems such as photovoltaic power generation equipment (e.g., encapsulant and backsheet). Photodegradation caused by ultraviolet (UV) radiation is the primary cause of failure for paints and coatings, as well as many other products made from polymeric materials that are exposed to sunlight. Other environmental variables including temperature and humidity can also affect degradation rates. When a new product that will be subjected to outdoor weathering is developed, it is necessary to assess the product's service life. As an example, for paints and coatings, the traditional method of service life prediction involves sending perhaps ten coated panels to Florida (where it is sunny and humid) and another ten panels to Arizona (where it is sunny and dry). Then every six months one panel is returned from each exposure location for detailed evaluation (e.g., to quantify chemical and physical changes over time). If the amount of

Keywords and phrases: Degradation, Nonlinear model, Random effects, Reliability, Service Life Prediction, UV exposure.

degradation is sufficiently small after, say, five years, the service life is deemed to be satisfactorily long.

The problem with the traditional method of service life prediction is that it takes too long to obtain the needed assessment (Martin et al. 1996). For many decades, accelerated tests (e.g., Nelson 1990) have been used successfully to assess the lifetime of products and components in environments that do not involve UV exposure. Accelerated tests for photodegradation are, however, more complicated. Non-scientific approaches to achieve acceleration of the degradation process by simply "speeding up the clock" in laboratory testing led to incorrect predictions. It is believed that the efforts failed for a combination of reasons including that UV lamps do not have the same spectral irradiance distribution as the sun and that varying all experimental factors simultaneously (the opposite of what would be done in a carefully designed experiment) does not provide useful information for modeling and prediction.

Scientists at the U.S. National Institute of Standards and Technology (NIST), in collaboration with scientists and engineers from companies and other organizations, conducted a multi-year research program to collect necessary data via scientifically-based laboratory accelerated tests that could be used to build statistical models and then to predict the service life of polymeric materials subjected to outdoor weathering. The main objective of this paper is to describe the statistical modeling and analysis of the laboratory accelerated test data collected at NIST, which incorporate physical and chemical knowledge of the degradation mechanism. We also generate predictions for specimens that were subjected to outdoor exposure where dynamic explanatory variables (i.e., time-varying covariates) although not controlled, were recorded.

While the details of the NIST experiments are described in Section 2, here we provide a brief introduction. The laboratory accelerated weathering tests were conducted using the NIST Simulated Photodegradation via High Energy Radiant Exposure (SPHERE), a device in which spectral UV wavelength, UV spectral intensity, temperature, and relative humidity (RH) can be controlled over time. Also, outdoor-exposure experiments were conducted on the roof of a NIST building in Maryland over different time periods. Both sets of experiments used a model epoxy coating. Chemical degradation was measured on both the laboratory accelerated test specimens and the outdoor-exposed specimens every few days using Fourier transform infrared (FTIR) spectroscopy. Longitudinal information on ambient temperature, RH, and the solar intensity and spectrum for outdoor-exposed specimens were carefully recorded at 12-minute intervals over the period of outdoor exposure.

We use the following major steps for the statistical modeling and prediction based on NIST data from photodegradation of polymeric materials. In these major steps, we combine physical/chemical knowledge and accelerated test data to build a model that can predict field performance.

1. *Use the accelerated test data and knowledge of the physics and chemistry of the degradation process to help identify the functional forms for the experimental variables as they relate to the degradation path model.*

2. *Use the identified functional forms and the accelerated test data to build a degradation path model linking the sample degradation paths and the experimental variables.*

3. *Use the identified model to generate predictions of degradation for given covariate histories.*

4. *To verify the effectiveness of the statistical models, compare predictions, based on the accelerated test degradation data and model, with observed degradation paths for outdoor-exposed specimens.*

5. *Use prediction intervals to quantify the statistical uncertainties associated with the outdoor degradation predictions.*

1.2. *Related Literature.* In this section, we review the general degradation literature. Lu and Meeker (1993) provided examples of models and analyses of degradation data. To speed up the degradation process and provide information in a more timely manner, accelerated degradation tests are commonly used (e.g., Chapter 12 of Nelson 1990). Potential accelerating variables include the use rate or aging rate of a product, exposure intensity, voltage stress, temperature, humidity, etc. Degradation processes are often affected by dynamic covariates. The cumulative damage model has been used to describe the effect that dynamic covariates have on degradation and failure-time processes (e.g., Bagdonavičius and Nikulin 2001, and Hong and Meeker 2010). Liao and Elsayed (2006) considered reliability inference for accelerated degradation testing under varying stress. Hong et al. (2015) and Xu et al. (2016) used dynamic covariates to build predictive models for degradation.

In recent years, new degradation analysis techniques have been developed using a functional data analysis framework. Zhou, Serban, and Gebraeel (2011) used functional data analysis approaches for degradation modeling and residual lifetime prediction. Zhou, Gebraeel, and Serban (2012) presented degradation modeling and monitoring based on truncated degradation signals using the framework of functional data analysis. Zhou et al. (2014) developed a functional time warping approach for degradation analysis. Zhou, Serban, and Gebraeel (2014) considered residual life prediction under different environments. Recent development of stochastic models for degradation analysis includes Wang and Xu (2010), Ye and Chen (2014), and Peng (2016), using the inverse Gaussian process as the main model. Pan and Crispin (2011) used a hierarchical modeling approach to analyze accelerated degradation testing data, and Wang et al. (2013) developed a Bayesian framework for degradation analysis. Zhang and Liao (2015) considered degradation modeling with a random degradation initiation time. Existing methods, however, can not be directly applied for the degradation modeling problem in this paper because photodegradation involves multiple accelerating variables under complicated relationships, and the outdoor prediction involves time-varying covariates.

In the area of photodegradation modeling, Gu et al. (2009) described three potential approaches to link laboratory accelerated degradation test data with outdoor-exposure data for a coating system. In a preliminary report of the NIST experimental program, Vaca-Trigo and Meeker (2009) described a predictive model to link the NIST laboratory accelerated test data and outdoor-exposure data. They used a nonlinear model for the accelerated test data and a cumulative damage model to predict the outdoor-exposure data. In this paper, we use a sophisticated nonlinear mixed-effects model with a careful physically-motivated modeling of the effects of the accelerating variables on the sample degradation paths. We also account for different sources of variability in the degradation path. The improved model in this paper provides enhanced prediction performance and the ability to quantify prediction uncertainty

with prediction intervals.

1.3. *Overview.* The rest of this paper is organized as follows. Section 2 describes the laboratory accelerated test and the outdoor-exposure experiments for data collection and provides notation for the data. Section 3 describes the nonlinear mixed-effects model and defines total effective dosage. Section 4 uses the laboratory accelerated test data to compute estimates of a categorical-effects model, providing information about the functional forms of the experimental variables needed to identify a model relating photodegradation to the experimental variables. Section 5 uses model parameter estimates from the laboratory accelerated test data and a cumulative damage model to predict outdoor-exposure degradation and compares the predictions with actual outdoor-exposure degradation paths. A comparison is also done for several different models in terms of model fitting and prediction accuracy. Section 6 contains conclusions and discussion of areas for future research.

2. Photodegradation Data.

2.1. *Laboratory Accelerated Test Experiments and Data.* We first briefly discuss the time scale for degradation processes. For a coating subjected to UV exposure, the scientifically appropriate time scale is proportional to the number of photons that get absorbed into the coating, taking into account that shorter wavelength photons are more energetic (and thus have a higher probability to cause damage). For those who study photodegradation, such a measure is called UV dosage, as will be described in detail in subsequent sections of this paper.

The light source for the laboratory accelerated test experiments was high-intensity UV lamps. The spectral irradiance of the lamps is a function of wavelength λ, which gives the power density at a particular wavelength λ. The spectral irradiance of the UV lamps in the NIST SPHERE is illustrated in Figure 1. Specifically, the irradiance is defined as the power of the electromagnetic radiation per unit area incident on a surface.

The effect of UV radiation on degradation depends on both the UV spectrum and UV intensity. UV radiation with shorter wavelengths tends to have higher energy per photon, thus causing more damage to the material when compared with UV radiation with longer wavelengths. Also, for the UV with the same wavelength, higher UV intensity (means more photons per time unit) tends to cause more damage than lower intensity. To study the effect of UV spectrum and UV intensity, the spectral irradiance of the lamps was modified and controlled by bandpass (BP) and neutral density (ND) filters. BP filters pass only UV with wavelengths over a particular range. For example, the 306 nanometer (nm) BP filter has a nominal center wavelength of 306 nm and full-width-half maximum values of ± 3 nm. The four BP filters used in the experiments have nominal center wavelengths of 306 nm, 326 nm, 353 nm, and 452 nm.

ND filters control the intensity of the UV radiation without affecting the shape of the UV spectrum. For example, a 10% ND filter (nominally) passes 10% of the UV photons at any wavelength. The four ND filters used in the experiments are 10%, 40%, 60%, and 100% (actually, a 100% ND would use no ND filter). As an illustration, Figure 2 shows all combinations of the 16 BP and ND filters.

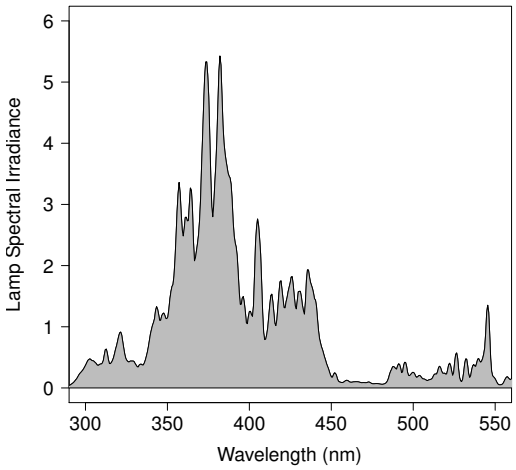

FIG 1. *Plot of the laboratory accelerated test lamp spectral irradiance distribution.*

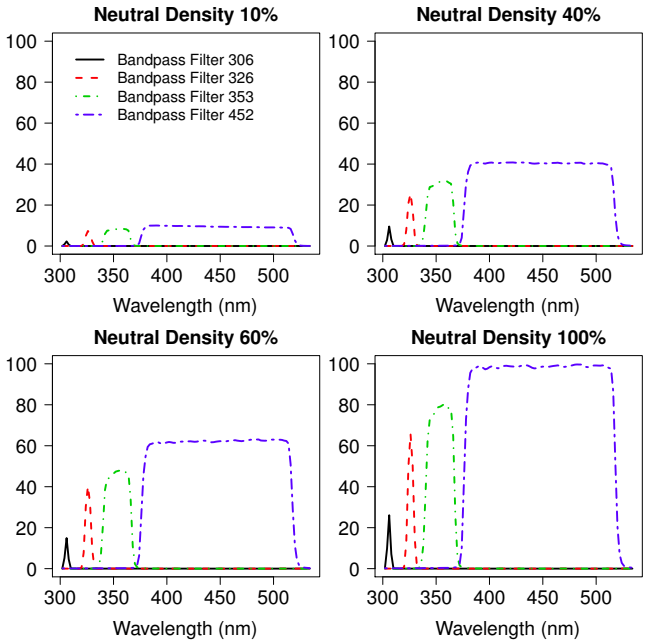

FIG 2. *Illustration of the combinations of the BP and ND filters. The y-axis shows the percentage of photons passing through the combinations of filters.*

TABLE 1
Laboratory accelerated test setup, showing the BP filters, ND filters, and levels of temperature and RH.

BP filter	306 nm (±3 nm), 326 nm (±6 nm), 353 nm (±21 nm), 452 nm (±79 nm)
ND filter	10%, 40%, 60%, 100%
Temperature	25°C, 35°C, 45°C, 55°C
RH	0%, 25%, 50%, 75%

TABLE 2
Summary of the 80 experimental combinations of BP and ND filters and temperature and RH levels. An empty cell implies that no experiments were done for the corresponding combination of temperature and RH. 4×4 implies that experiments were done for all of the 16 combinations of the BP and ND filters at the corresponding temperature and RH combination. 4×1 implies that experiments were done for all four BP filters and the 100% ND filters for the corresponding temperature and RH combination.

Temp \ RH	0%	25%	50%	75%
25	4×4			
35	4×4	4×1	4×1	
45		4×1	4×1	4×4
55				4×4

The laboratory accelerated test experiments also have other controlled environmental factors: temperature and RH. Table 1 gives a summary of the experimental factors for the laboratory accelerated degradation experiment. The temperature levels were 25°C, 35°C, 45°C, and 55°C. The RH levels were 0%, 25%, 50%, and 75%. The laboratory accelerated test data contain a total of 80 combinations of the experimental factors. Due to time and funding constraints, not all combinations of the four experimental factors were run in the experiments. Table 2 summarizes the 80 experiment combinations of the BP and ND filters, and temperature and RH levels. There were four replicates for most of the experimental factor-level combinations. A total of 319 specimens were exposed in the laboratory accelerated test experiments.

Damage to the material, which is used as an indication for degradation, was measured by Fourier transform infrared (FTIR) spectroscopy. An FTIR spectrometer provides an infrared spectrum of absorption or emission of a material. In particular, special structures of compounds absorb the infrared energy at different wavelengths, which results in peaks in the FTIR spectra. The locations of the FTIR peaks correspond to unique chemical structures and thus can be used to identify the relative concentration of different compounds. The height of a peak is proportional to the concentration of a particular compound or structure. The time intervals between the FTIR measurements in the accelerated test were typically on the order of a few days.

Figure 3 gives an illustration of FTIR peaks for a particular specimen at one point in time. Our modeling focuses on intensity changes at wavenumber 1250 cm^{-1}, which corresponds to C-O stretching of aryl ether. Other peaks that were recorded as potentially useful responses include 1510 cm^{-1} (benzene ring stretching), 1658 cm^{-1} (C=O stretching of oxidation products), and 2925 cm^{-1} (CH_2 stretching) (e.g., see

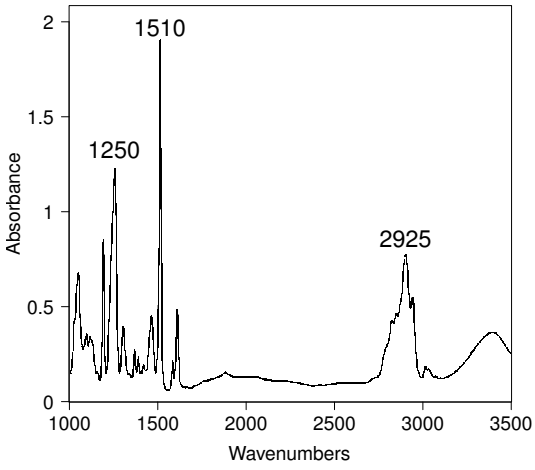

FIG 3. *Illustration of FTIR spectrum of the model epoxy used in the NIST experiments.*

Bellinger and Verdu 1984, Bellinger and Verdu 1985, Rabek 1995, and Kelleher and Gesner 1969).

As an example of the degradation data collected in the laboratory accelerated test experiments, Figure 4 shows the degradation paths for FTIR wavenumber 1250 cm^{-1} for specimens with 10%, 40%, 60% and 100% ND filters, the BP filter centered at 353 nm, temperature 35°C, and 0% RH. For this wavenumber, the degradation paths are decreasing (i.e., the amount of C-O stretching of aryl ether was decreasing). As expected, the degradation rates were higher for the ND filters passing larger percentages of UV photons. For the groups of two to four specimens exposed to the same conditions (and at the same time and in the same chamber), there is some specimen-to-specimen variability.

To use a degradation model to make inferences about failure times, it is necessary to have a definition of failure. When dealing with soft failures (as is commonly done in degradation analysis applications), such definitions generally have a subjective element (e.g., at what point in loss of gloss of a coating do we have a failure), but such decisions are typically made in a purposeful manner and with great care (e.g., using customer survey information to assess perception of gloss loss). These ideas relating degradation modeling to the estimation of service life are widely used in applications of degradation data modeling (e.g., the light output of lasers and LEDs, corrosion of pipelines, and growth of cracks in structures). During the NIST experimental program, physical measurements of gloss loss were also taken and correlated with the FTIR chemical degradation measurements. One reason that we choose to use the wavenumber 1250 cm^{-1} as our response is that it correlated best with gloss loss of the model epoxy used in the NIST experiments. As indicated by the horizontal lines in Figures 4 and 5, a damage level of -0.40 was used as the failure definition.

2.2. *Outdoor-Exposure Experiments and Data.* The UV exposure for the outdoor-exposure specimens is from the sun. There were 53 specimens in the outdoor-exposure

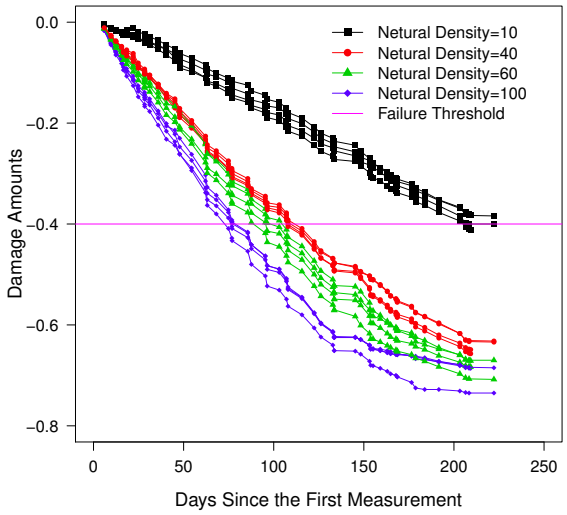

FIG 4. *Degradation paths for specimens with 10%, 40%, 60% and 100% ND filters, the 353 nm BP filter, temperature at 35° C, and 0% RH.*

experiments and they were exposed over different time intervals during a three-year period. The UV spectral irradiance, temperature, and RH are, of course, uncontrolled outside, but were recorded at 12-minute intervals. For the outdoor-exposure specimens, the UV, temperature, and RH are dynamic covariates. The measurements of degradation were taken every three to four days, similar to the accelerated test specimens. We continue to focus on chemical changes at the wavenumber 1250 cm^{-1}. Note, however, that we used the laboratory accelerated test data for model fitting. The data from the outdoor-exposed specimens are used only for validating the accelerated test methodology.

We also want to point out the interesting difference between the laboratory accelerated test data and outdoor-exposure data. The data shown in Figure 4 were collected in laboratory accelerated tests in which the UV, temperature, and RH are controlled to be constant over time. All of the sample paths have the same shape. Figure 5, on the other hand, shows the sample degradation paths as a function of the days since the beginning of exposure for a representative subset of 12 specimens that were exposed outdoors at different times. The sample degradation paths have different shapes, depending on the time of the year that the specimens were being exposed. The variability in the shapes of degradation paths for the outdoor-exposure data is due to and can be explained by the variability in the dynamic covariate time series (also see Hong et al. 2015).

To further illustrate and understand the outdoor-exposure degradation-path patterns, Figure 6(a) shows the degradation path for a particular outdoor-exposed specimen as a function of the calendar time. Figures 6(b), 6(c), and 6(d) show the dynamic covariates corresponding to the particular degradation path in Figure 6(a). From Figure 6(d), we can see that the UV intensity is low during the late fall and winter

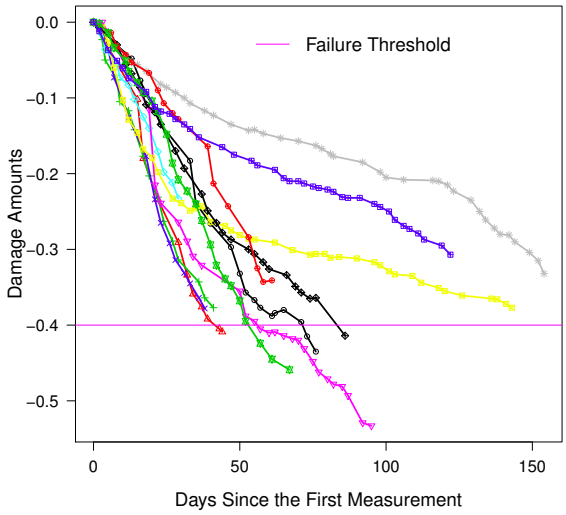

FIG 5. *Plots of the degradation paths as a function of the days since the first measurement for a representative subset of 12 outdoor-exposed specimens.*

months, corresponding to a smaller slope in the degradation path, while the UV is stronger for the months of March and April, corresponding to a larger slope in the degradation path.

2.3. *Notation.* Here we introduce notation for the data. The degradation (damage) measurement for specimen i is the change (relative to the value at the beginning of exposure) in the FTIR peak at 1250 cm^{-1} at time t_{ij} and for the laboratory accelerated test data is denoted by $y_i(t_{ij})$, $i = 1, \ldots, n$, $j = 1, \ldots, m_i$. Here, n is the total number of laboratory accelerated test specimens and m_i is the number of time points where the degradation measurements were taken for specimen i. The last observation time for specimen i is denoted by $t_i = t_{im_i}$.

For the laboratory accelerated test data, the UV radiation is quantified by the cumulative dosage $D_i(\tau_{il})$ at time τ_{il} (note that the cumulative dosage values were reported at times that differ from the times at which the degradation measurements were taken). The cumulative dosage is proportional to the total number of photons that were absorbed by specimen i across all wavelengths between time 0 and τ_{il}. Here, $i = 1, \ldots, n$, $l = 1, \ldots, n_i$, where n_i is the number of time points at which the total dosage was recorded for specimen i.

For the laboratory accelerated test specimens, the experimental factors are held constant at specified levels over time. We let BP_i, ND_i, Temp_i, and RH_i be the BP filter, ND filter, temperature, and RH levels, respectively, for specimen i. In summary, the laboratory accelerated test data are $\{y_i(t_{ij}), D_i(\tau_{il}), \text{BP}_i, \text{ND}_i, \text{Temp}_i, \text{RH}_i\}$ for $i = 1, \ldots, n$, $j = 1, \ldots, m_i$, and $l = 1, \ldots, n_i$.

For the outdoor-exposure data, we use subscript k to index the exposed specimens. The degradation measurement at time t_{kj} is denoted by $y_k(t_{kj})$, $k = 1, \ldots, q, j =$

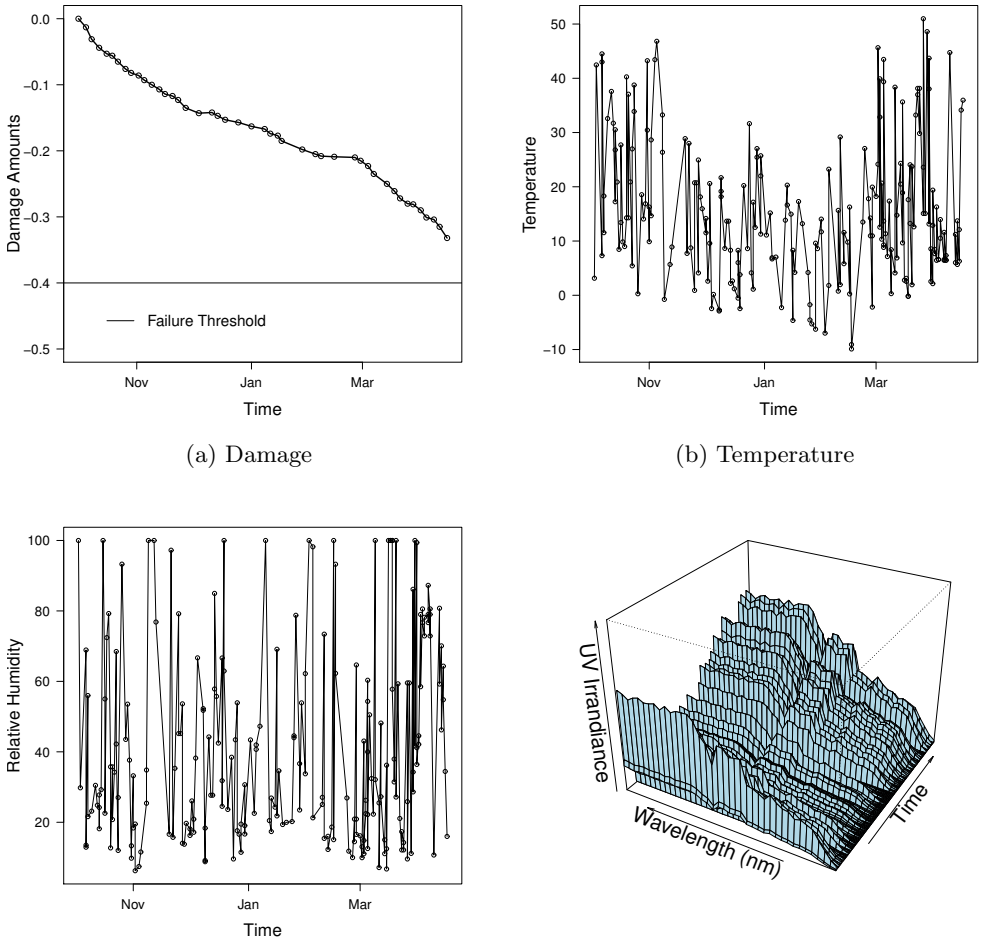

(a) Damage

(b) Temperature

(c) Relative humidity

(d) UV

FIG 6. *Plots of the degradation path for an outdoor-exposed specimen showing the relationship between the degradation and the dynamic covariates. (a) the degradation path, b) temperature as a function of time, c) RH as a function of time, and d) a perspective plot showing the recorded UV intensity as a function of time and wavelength.*

$1, \ldots, m_k$ for specimen k. Here q is the number of outdoor-exposure specimens. The recorded ambient temperature and RH for specimen k at time τ_{kl} are denoted by $\text{Temp}_k(\tau_{kl})$ and $\text{RH}_k(\tau_{kl})$, $l = 1, \ldots, n_k$, respectively. For the UV radiation, dosage was recorded for each 12-minute interval and each 2 nm wavelength interval between 300 nm and 532 nm. We denote the UV dosage for outdoor-exposure specimen k at time τ_{kl} and wavelength interval λ by $D_k(\tau_{kl}, \lambda)$. An example of $D_k(\tau_{kl}, \lambda)$ data is shown in Figure 6(d). In summary, the outdoor-exposure data are $\{y_k(t_{kj}), D_k(\tau_{kl}, \lambda), \text{Temp}_k(\tau_{kl}), \text{RH}_k(\tau_{kl})\}$ for $k = 1, \ldots, q$, $l = 1, \ldots, n_k$, and $j = 1, \ldots, m_k$.

3. Models for Photodegradation Paths.

3.1. *The Concept of UV Dosage.* The UV dosage is an important concept that will be used as the "time scale" for the subsequent photodegradation modeling. For the laboratory accelerated test data, only the cumulative dosage $D_i(\tau_{il})$ was available. Conceptually, the cumulative dosage is computed as follows. The number of incident photons from UV light source, defined as dose, for specimen i at time τ_{ik} from wavelength λ after BP and ND filters, is denoted by $E_i(\tau_{ik}, \lambda)$. Let $\text{Lamp}(\lambda)$ be the spectral irradiance of the UV lamp as a function of wavelength, and let $\text{Filter}(\lambda, \text{BP}_i, \text{ND}_i)$ denote the combined effect of the BP and ND filters. The dose $E_i(\tau_{ik}, \lambda)$ can be computed as

$$E_i(\tau_{ik}, \lambda) = E_i(\lambda) = \text{Lamp}(\lambda) \times \text{Filter}(\lambda, \text{BP}_i, \text{ND}_i),$$

which is constant over time for the laboratory accelerated test specimens due to the controlled experimental factors. The number of incident photons absorbed by a specimen at time τ_{ik}, defined as "dosage," is denoted by $D(\tau_{ik}, \lambda)$, where

$$D_i(\tau_{ik}, \lambda) = E_i(\tau_{ik}, \lambda)\{1 - \exp[-A(\lambda)]\},$$

and $A(\lambda)$ is the spectral absorbance of the specimen at specified wavelength λ (a property of the material). Thus, the cumulative dosage, which is proportional to the total number of photons absorbed by a specimen across all wavelengths up to time t, is computed as

$$D_i(t) = \int_0^t \int_\lambda D_i(\tau, \lambda) d\lambda d\tau,$$

where the integral is over the entire range of λ. We also define $D_{it}(\lambda) = \int_0^t D_i(\tau, \lambda) d\tau$ to be the wavelength-specific cumulative dosage.

3.2. *The Physical Model.* To model the effect of the experimental factors, we introduce the concept of "effective dosage." The cumulative effective dosage up to time t is defined as

$$\int_0^t \int_{\lambda_{\min}}^{\lambda_{\max}} D_i(\tau, \lambda) \phi(\lambda) d\lambda d\tau. \tag{1}$$

Here the function $\phi(\lambda)$ is the quasi-quantum yield function describing the fact that photons with a shorter wavelength have a higher probability of causing damage. The

wavelengths that are of interest are between $\lambda_{\min}$ and $\lambda_{\max}$. For values of $\lambda > \lambda_{\max}$, the probability of damage is negligible. For values of $\lambda < \lambda_{\min}$, potentially damaging photons are normally filtered out by the protective ozone layer in the stratosphere.

To allow for the environmental effects for specimen i, we use the following model for experimental-variable adjusted effective dosage.

$$S_i(t) = \int_0^t f(\text{Temp}_i) g(\text{RH}_i) d(\text{ND}_i) \int_{\lambda_{\min}}^{\lambda_{\max}} D_i(\tau, \lambda) \phi(\lambda) d\lambda d\tau. \tag{2}$$

Here $f(\text{Temp}_i)$, $g(\text{RH}_i)$ and $d(\text{ND}_i)$ are functions of the acceleration factors due to temperature, RH, and ND, respectively.

Dosage $D_i(\tau, \lambda)$ for each specimen was computed taking into account the nominal values of the ND filters. The percentage of UV photons passing through the ND filters, however, is not exactly equal to the nominal values. Thus the factor $d(\text{ND}_i)$ is used to provide a data-based adjustment for the deviations.

The quasi-quantum yield function $\phi(\lambda)$ describing the effect of UV spectrum is material dependent and unknown and needs to be estimated from the data. The estimation of $\phi(\lambda)$ from experimental data helps us understand material properties and how the UV exposure affects the degradation process at different wavelengths.

Environmental factors such as temperature and RH will also affect the degradation process. The Arrhenius relationship is widely used to describe the rate of chemical reactions and thus the acceleration effect of temperature. The manner in which RH and UV intensity (controlled by the neutral density filters) affect the degradation process, however, is unknown. That is, the functional forms of g and d need to be identified from a combination of scientific knowledge of the degradation process and the experimental data.

3.3. *The Statistical Model for Photodegradation.* In the general degradation path model, the degradation measurement of specimen i at time t_{ij} is

$$y_i(t_{ij}) = \mathcal{G}_i(t_{ij}) + \epsilon_i(t_{ij}), \tag{3}$$

where $\mathcal{G}_i(t_{ij})$ is the actual degradation path and $\epsilon_i(t_{ij})$ is the corresponding error term. Photodegradation is primarily driven by the effective dosage $S_i(t)$ as defined in (2). The general shape of the laboratory accelerated test degradation paths can be described by the following parametric model

$$\mathcal{G}_i(t_{ij}) = \frac{\alpha \exp(v_i)}{1 + \exp(-z)}, \tag{4}$$

where $z = \{\log[S_i(t_{ij})] - \mu\}/\sigma$, and μ and σ are the parameters describing the location and steepness of the damage curve, respectively. Ignoring the random effect v_i, the asymptote α reflects the maximum degradation damage when total effective dosage goes to infinity. The parameter $\exp(\mu)$ is the half-degradation effective dosage (i.e., the amount of effective dosage needed for the degradation to reach the level $\alpha/2$). The reciprocal of the scale parameter $1/\sigma$ is proportional to the slope of the degradation path for any fixed value of z. So a larger value of $1/\sigma$ implies a larger degradation rate.

In (4), the term v_i is the individual random effect for degradation path i, which is modeled by a normal distribution with mean 0 and variance σ_v^2. The random effect is used to explain the specimen-to-specimen variability that is caused by uncontrolled and/or unobservable factors (e.g., differences in fabricating the specimens or specimen position in the environmental chamber). The model in (4) is a nonlinear mixed-effects model. The statistical literature on this topic is rich. One can refer to, for example, Davidian and Giltinan (2003) or Pinheiro and Bates (2006) for more information about such models.

4. Modeling the Laboratory Accelerated Test Data.

4.1. *Initial Analysis of Laboratory Accelerated Test Data.* In this section, we perform some initial exploratory analyses of the laboratory accelerated test data. We start by fitting a categorical-effects model so that we can study the effects of the experimental variables without making any apriori assumptions about the form of the relationships. Because the experimental factors were held constant over time in the laboratory accelerated test, using the definition of $S_i(t_{ij})$ in (2), the term z in (4) can be computed as,

$$z = \frac{\log[S_i(t_{ij})] - \mu}{\sigma} = \frac{\log(t_{ij}) + \log[b(\mathrm{BP}_i)] + \log[f(\mathrm{Temp}_i)] + \log[g(\mathrm{RH}_i)] + \log[d(\mathrm{ND}_i)] - \mu}{\sigma}, \tag{5}$$

where

$$b(\mathrm{BP}_i) = \int_{\lambda_{\min}}^{\lambda_{\max}} \mathrm{Lamp}(\lambda)\mathrm{Filter}(\lambda, \mathrm{BP}_i, \mathrm{ND}_i)\{1 - \exp[-A(\lambda)]\}\phi(\lambda)d\lambda \tag{6}$$

is the effect of UV spectrum because it integrates over $\phi(\lambda)$ for the wavelength range defined by the BP_i.

For the model in (5), we use the constraint that $f(35) = g(25) = d(10) = 1$ to ensure that the parameters are estimable (i.e., we treat temperature 35°C, RH 25%, and ND 10% as the baseline experimental setting in the categorical-effects model). For the UV spectrum effect, only the values of $\log[b(\mathrm{BP}_i)] - \mu$ are estimable, which is sufficient because we are only interested in the relative relationship among the effects of the BP filters. The maximum likelihood (ML) estimates of parameters in (5) were obtained by using `nlme` in R. Degradation paths in a small wavelength interval [e.g., 306 nm (±3 nm)] have similar steepness. We assume σ is mainly determined by wavelength. Thus we denote the categorical effect by σ_λ for each of the four BP filters.

Table 3 lists the ML estimates of the fixed-effects parameters in (5). Although the categorical-effects model only provides estimates of the UV, temperature, and RH effects at a limited number of points, the information from the model is useful for guiding the choice of the functional forms of $\phi(\lambda)$, $d(\mathrm{ND})$, $f(\mathrm{Temp})$, $g(\mathrm{RH})$, and σ_λ in the next modeling stage.

4.2. *Effects of the Explanatory Variables.* In this section, we discuss the selection of the functional forms for the effects of explanatory variables used in the laboratory accelerated test.

TABLE 3
Parameter estimates for the categorical-effects model.

Parameter	Estimate	Standard Error	p-value
α	-0.6810	0.0130	< 0.0001
$\log[\bar{\phi}(306)] - \mu$	-6.5620	0.0755	< 0.0001
$\log[\bar{\phi}(326)] - \mu$	-7.0844	0.0361	< 0.0001
$\log[\bar{\phi}(353)] - \mu$	-9.0275	0.0323	< 0.0001
$\log[\bar{\phi}(452)] - \mu$	-10.1087	0.0350	< 0.0001
$\log[d(40)]$	-0.7939	0.0201	< 0.0001
$\log[d(60)]$	-1.0553	0.0199	< 0.0001
$\log[d(100)]$	-1.3082	0.0200	< 0.0001
$\log[f(25)]$	-0.1963	0.0092	< 0.0001
$\log[f(45)]$	0.1973	0.0247	< 0.0001
$\log[f(55)]$	-0.8193	0.0357	< 0.0001
$\log[g(0)]$	0.8749	0.0231	< 0.0001
$\log[g(50)]$	-0.3707	0.0255	< 0.0001
$\log[g(75)]$	0.2287	0.0240	< 0.0001
σ_{306}	1.5591	0.0149	< 0.0001
σ_{326}	1.2336	0.0074	< 0.0001
σ_{353}	1.0443	0.0057	< 0.0001
σ_{452}	0.8416	0.0054	< 0.0001

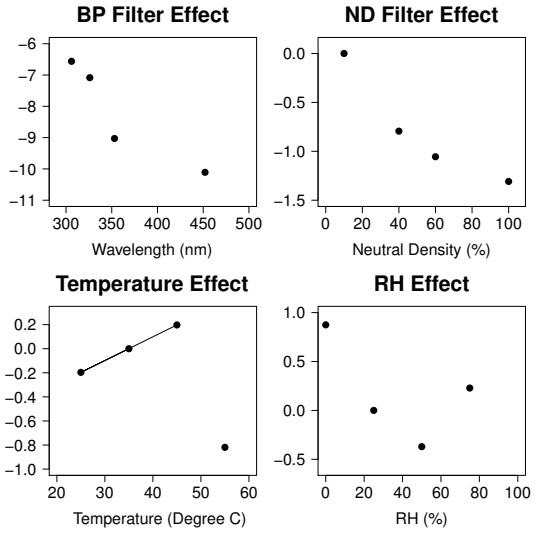

FIG 7. *Plots of the categorical effects for UV spectrum, ND filter, temperature, and RH.*

Modeling the BP Filter Effect. To suggest a functional form for $\phi(\lambda)$, we initially assume that $\phi(\lambda)$ is constant over the specific range of each BP filter, denoted by $\bar{\phi}(\lambda)$. For example, for the 306 nm BP filter, $\bar{\phi}(306)$ will be used to represent the effect. From (6), we obtain $b(\mathrm{BP}_i) = [D_i(t_i)/t_i]\bar{\phi}(\lambda)$. Because we record $D_i(t_i)$ and have an estimate of $b(\mathrm{BP}_i)$ from the categorical-effects model, we can obtain a heuristic estimate for $\bar{\phi}(\lambda)$ from this relationship. For example,

$$\bar{\phi}(306) = \frac{b(306)}{(\sum_{i:\mathrm{BP}_i=306}[D_i(t_i)/t_i])/(\sum_{i:\mathrm{BP}_i=306} 1)}, \tag{7}$$

for 303 nm $\leq \lambda \leq$ 309 nm. Similarly, one can obtain the estimates of $\bar{\phi}(\lambda)$ for the other BP filters, 320 nm $\leq \lambda \leq$ 332 nm, 332 nm $\leq \lambda \leq$ 374 nm, and 373 nm $\leq \lambda \leq$ 531 nm. The corresponding results are shown in Table 3. Figure 7(a) provides a visualization of a simple estimate of $\phi(\lambda)$. The results suggest that for shorter wavelengths, there is more damage than at longer wavelengths, agreeing with known physical theory.

The quasi-quantum yield $\phi(\lambda)$ describes the fact that photons at shorter wavelengths have higher energy and thus a higher probability of causing damage. Martin, Lechner, and Varner (1994) state that for polymeric materials, the shape of $\phi(\lambda)$ is typically exponential decay. The empirical results in our categorical-effects model also suggest this and thus we use a log-linear function $\phi(\lambda) = \exp(\beta_0 + \beta_\lambda \lambda)$, to describe quasi-quantum yield where β_0 and β_λ are parameters to be estimated from the data.

The parameter σ in (5) is related to the slope of the degradation path. Because UV is the main cause of degradation and shorter wavelength paths tend to have larger slopes, we model σ as a function of λ. The curve of categorical-effects estimates of σ_λ versus λ suggests an exponential relationship with a lower bound. Thus we use the functional form $\sigma_\lambda = \sigma_0 + \exp(\sigma_1 + \sigma_2\lambda)$ to describe the effect that UV wavelength has on σ.

From (5), one needs to have a wavelength specific dosage $D_{it}(\lambda)$ to estimate the parameters in $\phi(\lambda)$ (i.e., β_0 and β_λ). For the laboratory accelerated test data, however, only the aggregated dosage $D_i(t)$ data was available. We use an approximate method to obtain $D_{it}(\lambda)$ from $D_i(t)$. We consider the four intervals 303 nm $\leq \lambda \leq$ 309 nm, 320 nm $\leq \lambda \leq$ 332 nm, 332 nm $\leq \lambda \leq$ 374 nm, and 373 nm $\leq \lambda \leq$ 531 nm, corresponding to the four BP filters. Note that the spectral irradiance after filtering is $\mathrm{Lamp}(\lambda)\mathrm{Filter}(\lambda, \mathrm{BP}_i, \mathrm{ND}_i)$, and the approximate trapezoid area under each λ interval is denoted as Area_λ. The integration of Area_λ over each of the four wavelength intervals is denoted by $\mathrm{Area}_{\bar{\lambda}}$, where $\bar{\lambda}$ is 306 nm, 326 nm, 353 nm or 452nm, the BP filter nominal center points. We define the proportion of area under λ relative to its corresponding wavelength range as $P(\lambda) = \mathrm{Area}_\lambda/\mathrm{Area}_{\bar{\lambda}}$. Note that

$$D_i(t) = \int_0^t \int_\lambda \mathrm{Lamp}(\lambda)\mathrm{Filter}(\lambda, \mathrm{BP}_i, \mathrm{ND}_i)\{1 - \exp[-A(\lambda)]\} d\lambda d\tau, \tag{8}$$

and the specific form of $A(\lambda)$ is unknown. For the narrow intervals, 303 nm $\leq \lambda \leq$ 309 nm and 320 nm $\leq \lambda \leq$ 332 nm, we can assume $\{1 - \exp[-A(\lambda)]\}$ is constant because the fluctuation over the narrow range of wavelengths is relatively small. Thus, for 303 nm $\leq \lambda \leq$ 309 nm and 320 nm $\leq \lambda \leq$ 332 nm, we obtain approximate values from $D_{it}(\lambda) = D_i(t)P(\lambda)$. Although the interval 373 nm $\leq \lambda \leq$ 531 nm is wide, the

variation in $D_{it}(\lambda)$ will be small because both $\{1-\exp[-A(\lambda)]\}$ and $\phi(\lambda)$ are small over the interval. Thus we can assume that $D_{it}(\lambda)$ is constant for 373 nm $\leq \lambda \leq$ 531 nm. For the 332 nm $\leq \lambda \leq$ 374 nm, the lamp spectra curve is complicated and $\{1 - \exp[-A(\lambda)]\}$ is typically not small enough to do a trapezoidal approximation. Thus, in the subsequent modeling, we (as in the categorical-effects model) use $\bar{\phi}(353)$ to represent the effect of the 353 nm BP filter and treat it as an unknown parameter to be estimated from the data. There is, however, enough information from the other three BP filters for us to estimate the unknown parameters of the log-linear relationship for $\phi(\lambda)$.

ND Filter Effect. A power law relationship is typically used to describe the ND effect (e.g., James 1997). The power law relationship is based on Schwarzschild's law, which says that the photo-response of radiation over a given time period has a form ND^p, where ND is the UV intensity level. To achieve the same photo-response, $\mathrm{ND}^p \times t$ should be the same, where p is the Schwarzschild coefficient and t is the exposure time. When $p = 1$, this relationship is called the reciprocity law. Experimental deviations from the reciprocity law are called reciprocity law failure. More discussion about Schwarzschild's law and reciprocity can be found in Martin, Chin, and Nguyen (2003).

Figure 7(b) shows the effects of the ND filter. A power law relationship $d(\mathrm{ND}_i) = {\mathrm{ND}_i}^p$ gives a perfect fit to the four points. Note that the $\mathrm{Filter}(\lambda, \mathrm{BP}_i, \mathrm{ND}_i)$ already includes the effect of the ND filter as ND_i with a power of one. Thus, the overall effect of ND filter is ${\mathrm{ND}_i}^{(1+p)}$. If the reciprocity law (i.e., the effect of ND is ${\mathrm{ND}_i}^1$) holds, p should be equal to zero in this parameterization. Thus, combining the physical knowledge and the empirical evidence, we used the power law relationship to describe the UV intensity effects. Another way of thinking about this is that with the reparameterization, the effect p describes the deviation between the nominal properties of the ND filters and the actual amount of photon attenuation provided by the ND filters.

Temperature Effect. Figure 7(c) shows the effect that temperature has on the degradation rate. The Arrhenius relationship is widely used to describe the acceleration effect of temperature on the rate of a chemical reaction (e.g., Meeker, Escobar, and Lu 1998). According to the Arrhenius relationship, the logarithm of the reaction rate should be proportional to reciprocal temperature in the Kelvin scale. In particular, the Arrhenius relationship is

$$f(\mathrm{Temp}_i) = \gamma_0 \exp\left(\frac{-E_a/R}{\mathrm{TempK}_i}\right), \tag{9}$$

where TempK_i is the Kelvin temperature computed as Celsius temperature plus 273.15, E_a is the effective activation energy, and $R = 8.314\,\mathrm{J\,K^{-1}\,mol^{-1}}$ is a gas constant. We define E_a/R to be the temperature effect to be estimated from the data. The categorical-effects estimates agree well with this relationship except for the specimens at 55°C and 75 % RH.

A possible explanation for the change in the estimated temperature effect at 55°C is that there is an interaction between the high temperature and the high RH level. Such an interaction could arise because water release is known to affect the rate of degradation. We can not, however, estimate the interaction effect because there is data

at 55°C for only one RH level. Another possible explanation is that there had been a failure of an integrated circuit chip in a controller that caused certain chambers to be overheated for a period of time. This could have lead to a different failure mechanism for the affected specimens. Based on these considerations, we still use the Arrhenius relationship to model the temperature effect after removing the data at 55°C and 75% RH.

RH Effect. The effect of relative humidity on coating degradation is complicated. There are few theoretical results to suggest the functional form for humidity effect in this type of application. It is known that low humidity will accelerate the side-chain scission process. As more end groups are created, the degradation rate will tend to increase. On the other hand, higher water content in the coating (caused by higher levels of RH) will tend to increase the diffusion rate of oxygen in the oxidation zone, which can also increase the degradation rate (e.g., Chen and Fuller 2009, and Kiil 2009). Thus, there is a middle range of RH values where the degradation rate would be expected to be smaller than the rates at the extremes. These mechanisms suggest a hump shape function for the effect that RH has on degradation. Figure 7(d) shows the categorical-effects model estimates for the RH effect. The effect is increasing first and then decreasing, suggesting a concave relationship. Based on the empirical evidence and the suspected chemical reaction mechanisms, we used a quadratic model

$$\log[g(\mathrm{RH})] = -\beta_{\mathrm{RH}}(\mathrm{RH} - \mathrm{rh}_0)^2 \tag{10}$$

to describe the RH effect. Here, β_{RH} and rh_0 are unknown parameters to be estimated from the data.

4.3. *The Combined Model.* Combining all of the identified functional forms for the effects of the experimental variables gives following model for the underlying degradation path,

$$\mathcal{G}_i(t_{ij}) = \frac{\alpha \exp(v_i)}{1 + \exp(-z)}, \tag{11}$$

where

$$z = \frac{\eta_0 + \log[D_i(t_{ij})] + A + p(\log[\mathrm{ND}_i]) - \left(\frac{E_a/R}{\mathrm{TempK}_i}\right) - \beta_{\mathrm{RH}}\left(\mathrm{RH}_i - \mathrm{rh}_0\right)^2}{\sigma_0 + \exp(\sigma_1 + \sigma_2\lambda)},$$

$$A = \log\left[\int_{\lambda_{\min}}^{\lambda_{\max}} P(\lambda)\exp(\beta_\lambda \lambda) d\lambda\right],$$

and v_i is the random effect with mean 0 and variance σ_v^2. Note that the total effective dosage for wavelength λ is $S_i(t,\lambda) = D_{it}(\lambda)\exp(\beta_0 + \beta_\lambda\lambda)$, which is proportional to $D_{it}(\lambda)\exp(\beta_\lambda\lambda)$. We use $D_i(t) \times P(\lambda) \times \exp(\beta_\lambda\lambda)$ to approximate $D_{it}(\lambda)\exp(\beta_\lambda\lambda)$. We define the constant $\eta_0 = \beta_0 + \log(\gamma_0) - \mu$ because the μ and the individual intercept terms are not independently estimable in the model.

Table 4 lists the ML estimates of the parameters in (11). The maximum degradation damage when total effective dosage goes to infinity is -0.6191, not considering random

TABLE 4
Parameter estimates for the combined model in (11).

Parameter	Estimate	Standard Error	p-value
α	-0.6191	0.01013	< 0.0001
β_λ	-0.0297	0.00026	< 0.0001
p	-0.5606	0.00781	< 0.0001
$\frac{E_a}{R}$	1945.6482	75.83458	< 0.0001
β_{RH}	-0.0005	0.00001	< 0.0001
rh_0	45.4748	0.28749	< 0.0001
η_0	9.8986	0.25662	< 0.0001
$b(353)$	-11.5661	0.09428	< 0.0001
σ_0	0.8019	0.00664	< 0.0001
σ_1	7.6776	0.18760	< 0.0001
σ_2	-0.0260	0.00062	< 0.0001

effects. For the ND filter effect, the power p is estimated to be -0.5606, which is significantly different from 0. Thus there is evidence that the reciprocity law does not hold in this application. The combined ND effect in $\mathrm{Filter}(\lambda, \mathrm{BP}_i, \mathrm{ND}_i)$ is $1 - 0.5606 = 0.4394$. That is, $\mathrm{ND}^{0.4394}$ describes the overall effect of the ND filters. For example, the effect of a nominal 80% ND filter is $100(0.80^{0.4394})\% = 90.6\%$ filtering. As expected, the quasi-quantum yield coefficient $\beta_\lambda = -0.0297 < 0$ indicating that shorter wavelengths cause more damage. The estimate of E_a/R is 1945.6482. Thus the point estimate of the effective activation energy E_a is 234.0207. The estimate for the variance of random effects is $\widehat{\sigma}_v^2 = 0.058$. Figure 8 displays examples of our model (11) fitted to the laboratory accelerated test data, showing good agreement.

5. The Prediction Model for Outdoor-Exposure Data. In this section, we adapt the laboratory accelerated test model (11) and its parameter estimates to predict outdoor-exposure degradation.

5.1. *The Cumulative Damage Model for Outdoor-Exposure Degradation Prediction.* For computational convenience, we used 60 minutes instead of 12 minutes as the time interval for the dynamic covariates. For outdoor-exposure specimen k, we define the incremental effective dosage at wavelength interval $\lambda \pm 1$ over the 60-minute interval starting at τ to be

$$\Delta S_k^*(\tau, \lambda) = \int_{\tau}^{\tau+60\ \mathrm{min}} \int_{\lambda-1\,\mathrm{nm}}^{\lambda+1\,\mathrm{nm}} D_k(\tau, \lambda) \exp(\beta_\lambda \lambda) d\lambda d\tau. \tag{12}$$

Here we use an "$*$" to indicate that the difference from the effective dosage defined previously. The previous definition used $\phi(\lambda)$ but here we use $\exp(\beta_\lambda \lambda)$, which is proportional to $\phi(\lambda)$. The effective dosage across all wavelengths at time τ is $S_{k\tau}^*(\tau) = \int_\lambda \Delta S_k^*(\tau, \lambda) d\lambda$. The cumulative total effective dosage across all wavelengths from time 0 to time t is $S_k^*(t) = \int_0^t S_{k\tau}^*(\tau) d\tau$. Temperature and RH are averaged over all 60-minute intervals. Because no ND filters were used during the outdoor exposures, we set ND to be 100% for all outdoor-exposure predictions.

According to the cumulative damage model, the slope of the degradation curve at time τ and wavelength λ is a function of total effective dosage $S_k^*(\tau)$ and other

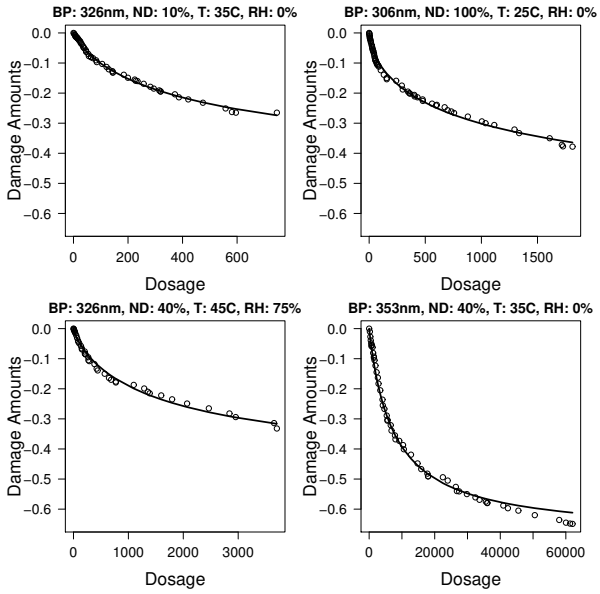

FIG 8. *Fitted degradation paths for four randomly selected specimens based on the model in* (11). *The points are the measured values and the lines show the fitted values. The plot titles show the levels of the experimental factors.*

environmental effects. That is,

$$g'_k(\tau,\lambda) = \frac{d\mathcal{G}_k(\tau)}{d[S^*_k(\tau)]} = \frac{1}{S^*_k(\tau)\sigma_\lambda} \times \frac{\alpha \exp(z)}{[1+\exp(z)]^2}, \tag{13}$$

where

$$z = \frac{\log[S^*_k(\tau)] + \eta_0 + p[\log(\mathrm{ND})] - \left[\frac{E_a/R}{\mathrm{Temp}_k(\tau)+273.15}\right] - \beta_{\mathrm{RH}}\left[\mathrm{RH}_k(\tau) - \mathrm{rh}_0\right]^2}{\sigma_0 + \exp\left(\sigma_1 + \sigma_2\lambda\right)}. \tag{14}$$

Note that here we compute the slope $g'_k(\tau,\lambda)$ as a function of τ and λ because σ_λ depends on λ and the incremental damage amounts need to be accumulated across the time τ and wavelength λ intervals. The incremental damage, $\Delta\mathcal{G}_k(\tau,\lambda)$, is the damage at time τ that was caused by the UV radiation in the 2nm wavelength interval $(\lambda-1,\lambda+1)$. In particular, $\Delta\mathcal{G}_k(\tau,\lambda) = g'_k(\tau,\lambda)\Delta S^*_k(\tau,\lambda)$. The additivity law is assumed, implying that the damage can be summed up from each wavelength interval in every 60-minute time interval. Then $\Delta\mathcal{G}_k(\tau)$ denotes incremental damage at time τ from all wavelengths, $\Delta\mathcal{G}_k(\tau) = \sum_\lambda \Delta\mathcal{G}_k(\tau,\lambda)$. The cumulative damage $\mathcal{G}_k(t)$ from time 0 to t from all wavelengths is

$$\mathcal{G}_k(t) = \sum_{\tau=0}^{t} \Delta\mathcal{G}_k(\tau). \tag{15}$$

Hence, the degradation level $\mathcal{G}_k(t)$ can be predicted based on the model estimated from the laboratory test data. Because there is a random effect v_k in the mean structure $\mathcal{G}_k(t)$, for the point prediction, we set v_k to be zero when computing point predictions.

5.2. *Outdoor-Exposure Prediction Uncertainty Quantification.* Here we use $\boldsymbol{\theta}$ to denote all the parameters in (11), and $\widehat{\boldsymbol{\theta}}$ is the ML estimator. The corresponding variance-covariance matrix is denoted by $\Sigma_{\widehat{\boldsymbol{\theta}}}$. The outdoor exposure prediction involves two sources of variability: the random effect v_k and the variability in $\widehat{\boldsymbol{\theta}}$. We use prediction intervals to quantify the prediction uncertainty. Prediction intervals are calculated and calibrated following a procedure that is similar to those described in Hong, Meeker, and McCalley (2009), using the Lawless and Fredette (2005) predictive distribution. For notational simplicity, let $\mathcal{G} = \mathcal{G}_k(t)$, because we compute pointwise prediction intervals. The cumulative distribution function of $\mathcal{G}$ at a particular point in time t is denoted by $F(\mathcal{G}; \boldsymbol{\theta})$ which is primarily determined by the distribution of the random effect. The algorithm to compute the predictive distribution is as follows.

1. Simulate B sample estimates $\widehat{\boldsymbol{\theta}}_b^* \sim \mathrm{N}(\widehat{\boldsymbol{\theta}}, \Sigma_{\widehat{\boldsymbol{\theta}}})$ and $v_b^* \sim \mathrm{N}(0, \widehat{\sigma}_v^2), b = 1, \ldots, B$. We use $B = 50{,}000$.
2. Compute the degradation $\mathcal{G}_b^*, b = 1, \ldots, B$ using the method summarized by (15) under parameter $\widehat{\boldsymbol{\theta}}_b^*$ and the random effect v_b^*.
3. Compute $W_b^* = F(\mathcal{G}_b^* | \widehat{\boldsymbol{\theta}}_b^*), b = 1, \ldots, B$.
4. Compute w^l and w^u, the lower and upper $\alpha/2$ sample quantiles, respectively, of W_b^*.
5. Solve $F(\mathcal{G}^l | \widehat{\boldsymbol{\theta}}) = w^l, F(\mathcal{G}^u | \widehat{\boldsymbol{\theta}}) = w^u$ for $(\mathcal{G}^l, \mathcal{G}^u)$, providing the $100(1-\alpha)\%$ calibrated prediction interval.

This algorithm needs to be repeated over the range of t values of interest.

5.3. *Outdoor-Exposure Prediction Results and Model Comparisons.*

Outdoor-Exposure Predictions. Figure 9 compares the measured and predicted degradation paths based on our cumulative damage model for the same representative set of outdoor-exposed sample paths shown in Figure 5. The predicted values for some specimens agree well with the measured values, while for others the predicted values are either above or below that of the actual outdoor-exposed sample paths. These variations correspond to the distribution of the random effects. Most of the measured data points are within the calibrated prediction intervals, except for some small levels of degradation at early times which may have been caused by measurement error. Because the random effects are modeled as normally distributed with mean 0, the average predicted values should be close to the averaged measured values for all 53 outdoor-exposed specimens. Figure 10 shows the average of predicted and measured damage for all of the outdoor-exposed specimens. The average predicted values correspond well to average measured values.

We saw that the random effects tend to be similar within the same outdoor-exposed group. For example, four specimens from outdoor-exposed group G1 all have predictions larger than the measured values. The four specimens from group G16OUT all have predictions smaller than the measured values, and the four specimens from group G4 all have predictions close to the measured values. These suggest that the random effects could be related to group conditions such as additional weather-related effects not accounted for in our model. Other factors that may contribute to the random effects include the non-uniform spatial irradiance of specimens, possible non-uniformity of the material of the specimens, etc.

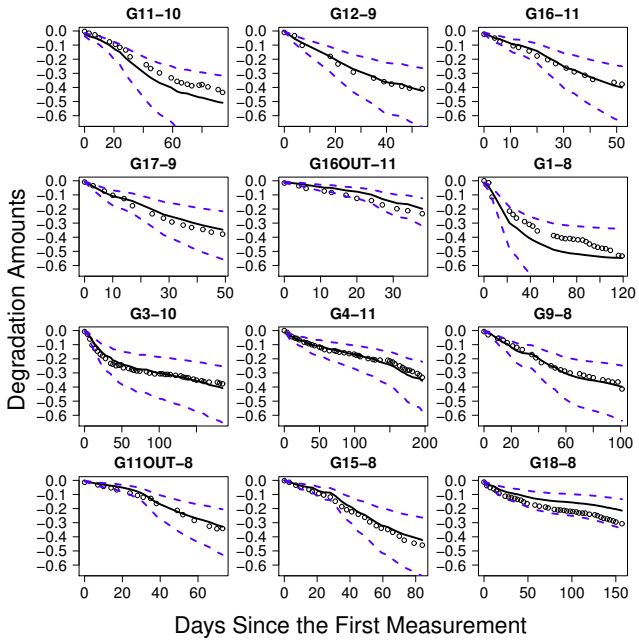

FIG 9. *Prediction results for 12 representative outdoor-exposed specimens. The points show the measured values, the solid lines show the predicted values, and the dashed lines show the 95% pointwise prediction intervals.*

Predictions with Early Degradation Information. When information about the early part of degradation path is available for a particular specimen k, that information can be used to estimate the random effect v_k, providing a more precise prediction of the future amount of degradation. Such predictions are often needed in practice (say for a fleet of units in the field or for individual units) to estimate the distribution of the remaining life. In particular, we used the fifth to tenth data points and use the least squares approach to find $\widehat{v}_k$. That is $\widehat{v}_k$ is the value that minimizes $\sum_{j=5}^{10}[y_{kj} - \exp(v_k)\widehat{y}_{kj}]^2$, where $\widehat{y}_{kj}$ is obtained by substituting the ML estimates into the prediction model. Then the predicted path for specimen k is obtained as $\exp(\widehat{v}_k)\widehat{y}_{kj}$. The first four data points were not used because their damage values were too small (i.e., the damage amount is less than 0.01) to be useful in estimating v_k. Figure 11 shows the results for several example specimens where we estimated random effect $\exp(v_k)$ using the early part of the degradation. The dashed lines indicate the predicted values after adjusting. For most specimens, the adjusted predicted values match the measured values considerably better than the unadjusted values.

Comparisons. This section describes comparisons among several models. We used the Akaike information criterion (AIC) for model-fitting comparisons and the mean squared error (MSE) for prediction comparisons. We considered the following models for comparisons.

- Model A: A model similar to that was used in Vaca-Trigo and Meeker (2009), using no random effect and where UV intensity was not modeled directly.
- Model B: The model in (4) with individual random effects for each specimen and

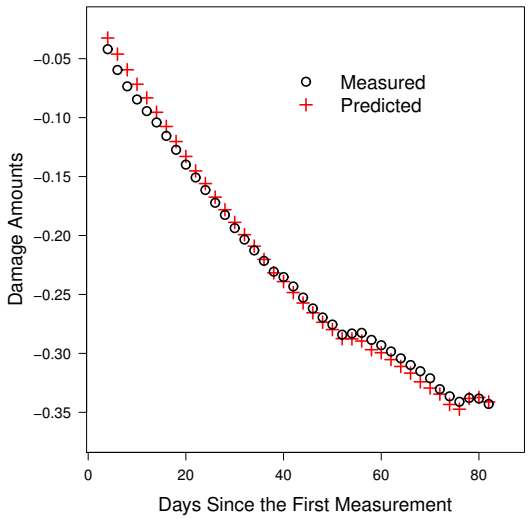

FIG 10. *Plots of averaged outdoor-exposed degradation measurements and values predicted by the cumulative damage model.*

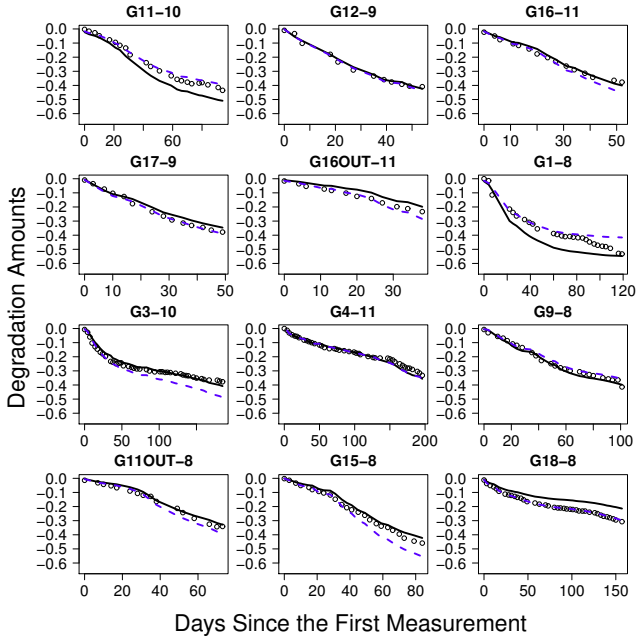

FIG 11. *Prediction results for 12 representative outdoor-exposed specimens, with adjustment made by random effects estimated from the 5th to 10th data points. The points show the measured values, the solid lines show the predictions without adjustments, and the dashed lines show the predictions with adjustments.*

TABLE 5
Comparisons of model fits and predictions.

Model	Log likelihood values	Number of parameters	AIC	Prediction	
				Model	MSE
A	15740.22	9	−31462.44	A	0.004238
B	30201.98	13	−60377.95	B1	0.002879
				B2	0.002522
C	30414.43	14	−60800.85	C1	0.002524
				C2	0.002396

carefully modeled effects for all of the experimental variables. For predictions from this model, there are two variants.

  - Model B1: Prediction with all random effects set equal to the expected value of zero.
  - Model B2: Prediction using some of the early data points to estimate the random effects for the individual specimens.

- Model C: The model in (4) can be easily extended to more complicated random-effects structures. For Model C, we consider the model in (4) but with both specimen-to-specimen and group-to-group random effects. Note that there were typically four replicates within experimental group (i.e., exposed at the same time and in the same chamber). For predictions from this model, we also have two variants.
  - Model C1: Prediction with all random effects set equal to the expected value of zero.
  - Model C2: Prediction using some of the early data points to estimate the random effects for the groups and the individual specimens.

Table 5 shows the model comparison results. The results show that the proposed Models B and C provide a much better fit to the laboratory accelerated test data than the model in Vaca-Trigo and Meeker (2009). There is not much difference between the prediction performance of Models B and C. Both models provide much better predictions than Model A.

6. Conclusions and Areas for Future Research. This paper describes the statistical modeling and analysis of accelerated test data for photodegradation and the prediction of photodegradation for specimens subjected to outdoor exposure. We used a physically motivated nonlinear regression model with random effects to describe the laboratory accelerated test degradation data, carefully studied the functional forms of the experimental variables to develop the model, and estimated model parameters from the accelerated test data. We found that the log-linear relationship and the power law relationship can provide adequate descriptions of the effects of UV spectrum and intensity, respectively. The Arrhenius relationship can describe the temperature effects well, and the quadratic relationship can describe the RH effect well.

We used a cumulative damage model, incorporating the parameter estimates from the laboratory accelerated test and individual specimen dynamic covariate information, to predict the individual outdoor-exposed degradation paths. We also developed

an algorithm to calculate prediction intervals. The outdoor predictions agree well with the observed degradation, indicating that both indoor and outdoor degradation share the same degradation mechanism. The comparison results show that the models in this paper provide a much better fit to the laboratory accelerated test data, and more accurate outdoor prediction than the results in Vaca-Trigo and Meeker (2009), which indicates that the model improvements in this paper are important for better photodegradation modeling and prediction.

Although NIST has been a leader in the development of UV accelerated test methods, UV testing is quite common in industry, and UV testing equipment is readily available from companies like Atlas (http://atlas-mts.com/). Also, because photodegradation is common for polymeric materials, such as components used in photovoltaic panels, the results in this paper will be useful to statisticians and engineers working in this area. Although the analysis in this paper is based on the data collected from a model epoxy, the modeling and prediction methods can also be used to predict the degradation of other materials such as ethylene-vinyl acetate (EVA) and polyethylene terephthalate (PET) and materials containing UV protection.

The degradation modeling and prediction methods presented in this paper serve as an important step in the development of the science of outdoor weathering service life prediction. There are, however, several areas for further research. Given a probability model for degradation paths and corresponding random effects, a specific set of dynamic-covariate time series, and a definition of the corresponding soft-failure threshold, methods need to be developed to compute the failure-time distribution for exposed units. In general, outdoor environments are complicated, and a more extensive experiment could be conducted to study the effect of factors like contaminants in the air, dust, acid rain, and extreme weather events. In recent years, new degradation analysis methods have been developed such as functional data analysis approach (e.g., Zhou et al. 2014, and Zhou, Serban, and Gebraeel 2014) and stochastic models (e.g., Peng 2016). The extension of existing methods for photodegradation analysis will be an interesting area for future research.

Acknowledgments. The authors thank the editor, an associate editor, and the referees, for their valuable comments that lead to significant improvement on this paper. The authors acknowledge Advanced Research Computing at Virginia Tech for providing computational resources. The work by Hong was partially supported by the National Science Foundation under Grant CMMI-1634867 to Virginia Tech.

References.

Bagdonavičius, V. and M. S. Nikulin (2001). Estimation in degradation models with explanatory variables. *Lifetime Data Analysis 7*, 85–103.

Bellinger, V. and J. Verdu (1984). Structure-photooxidative stability relationship of amine-crosslinked epoxies. *Polymer Photochem 5*, 295–311.

Bellinger, V. and J. Verdu (1985). Oxidative skeleton breaking in Epoxy-Amine networks. *Journal of Applied Polymer Science 30*, 363–374.

Chen, C. and T. F. Fuller (2009). The effect of humidity on the degradation of Nafion membrane. *Polymer Degradation and Stability 94*, 1436–1447.

Davidian, M. and D. M. Giltinan (2003). Nonlinear models for repeated measurement data: An overview and update. *Journal of Agricultural, Biological, and Environmental Statistics 8*, 387–419.

Gu, X., B. Dickens, D. Stanley, W. Byrd, T. Nguyen, I. Vaca-Trigo, W. Q. Meeker, J. Chin, and J. Martin (2009). Linking accelerating laboratory test with outdoor performance results for a model epoxy coating system. In J. W. Martin, R. A. Ryntz, J. Chin, and R. A. Dickie (Eds.), *Service Life Prediction of Polymeric Materials, Global Perspectives*, pp. 3–28. NY: New York: Springer.

Hong, Y., Y. Duan, W. Q. Meeker, X. Gu, and D. Stanley (2015). Statistical methods for degradation data with dynamic covariates information and an application to outdoor weathering data. *Technometrics 57*, 180–193.

Hong, Y. and W. Q. Meeker (2010). Field-failure and warranty prediction based on auxiliary use-rate information. *Technometrics 52*, 148–159.

Hong, Y., W. Q. Meeker, and J. D. McCalley (2009). Prediction of remaining life of power transformers based on left truncated and right censored lifetime data. *The Annals of Applied Statistics 3*, 857–879.

James, T. (1997). *The Theory of the Photographic Process* (fourth ed.). New York: Macmillan.

Kelleher, P. and B. Gesner (1969). Photo-oxidation of phenoxy resin. *Journal of Applied Polymer Science 13*, 9–15.

Kiil, S. (2009). Model-based analysis of photoinitiated coating degradation under artificial exposure conditions. *Journal of Coatings Technology and Research 9*, 375–398.

Lawless, J. F. and M. Fredette (2005). Frequentist prediction intervals and predictive distributions. *Biometrika 92*, 529–542.

Liao, H. and E. A. Elsayed (2006). Reliability inference for field conditions from accelerated degradation testing. *Naval Research Logistics 53*, 576–587.

Lu, C. J. and W. Q. Meeker (1993). Using degradation measures to estimate a time-to-failure distribution. *Technometrics 34*, 161–174.

Martin, J. W., J. W. Chin, and T. Nguyen (2003). Reciprocity law experiments in polymeric photodegradation: a critical review. *Progress in Organic Coatings 47*, 292–311.

Martin, J. W., J. A. Lechner, and R. N. Varner (1994). Quantitative characterization of photodegradation effects of polymeric materials exposed in weathering environments. In W. D. Ketola and D. Grossman (Eds.), *Accelerated and Outdoor Durability Testing of Organic Materials, ASTM-STP-1202*. Philadelphia: American Society for Testing and Materials.

Martin, J. W., S. C. Saunders, F. L. Floyd, and J. P. Wineburg (1996). Methodologies for predicting the service lives of coating systems. In D. Brezinski and T. Miranda (Eds.), *Federation Series on Coating Technology*, pp. 1–32. Blue Hill, PA: Federation Series on Coating Technology.

Meeker, W. Q., L. A. Escobar, and C. J. Lu (1998). Accelerated degradation tests: modeling and analysis. *Technometrics 40*, 89–99.

Nelson, W. (1990). *Accelerated Testing: Statistical Models, Test Plans, and Data Analyses*. New York: John Wiley & Sons.

Pan, R. and T. Crispin (2011). A hierarchical modeling approach to accelerated

degradation testing data analysis: A case study. *Quality and Reliability Engineering International 27*, 229–237.

Peng, C.-Y. (2016). Inverse Gaussian processes with random effects and explanatory variables for degradation data. *Technometrics 57*, 100–111.

Pinheiro, J. and D. Bates (2006). *Mixed-effects models in S and S-PLUS*. NY: New York: Springer Science & Business Media.

Rabek, J. (1995). *Polymer Photodegradation-Mechanisms and Experimental Methods*. London, UK: Chapman & Hall.

Vaca-Trigo, I. and W. Q. Meeker (2009). A statistical model for linking field and laboratory exposure results for a model coating. In J. Martin, R. A. Ryntz, J. Chin, and R. A. Dickie (Eds.), *Service Life Prediction of Polymeric Materials*, pp. 29–43. New York, NY: Springer.

Wang, L., R. Pan, X. Li, and T. Jiang (2013). A Bayesian reliability evaluation method with integrated accelerated degradation testing and field information. *Reliability Engineering & System Safety 112*, 38–47.

Wang, X. and D. Xu (2010). An inverse Gaussian process model for degradation data. *Technometrics 52*, 188–197.

Xu, Z., Y. Hong, and R. Jin (2016). Nonlinear general path models for degradation data with dynamic covariates. *Applied Stochastic Models in Business and Industry 32*, 153–167.

Ye, Z.-S. and N. Chen (2014). The inverse Gaussian process as a degradation model. *Technometrics 56*, 302–311.

Zhang, Y. and H. Liao (2015). Analysis of destructive degradation tests for a product with random degradation initiation time. *IEEE Transactions on Reliability 64*, 516–527.

Zhou, R., N. Gebraeel, and N. Serban (2012). Degradation modeling and monitoring of truncated degradation signals. *IIE Transactions 44*, 793–803.

Zhou, R., N. Serban, and N. Gebraeel (2014). Degradation-based residual life prediction under different environments. *Annals of Applied Statistics 8*, 1671–1689.

Zhou, R., N. Serban, N. Gebraeel, and H.-G. Müller (2014). A functional time warping approach to modeling and monitoring truncated degradation signals. *Technometrics 56*, 67–77.

Zhou, R. R., N. Serban, and N. Gebraeel (2011). Degradation modeling applied to residual lifetime prediction using functional data analysis. *The Annals of Applied Statistics 5*, 1586–1610.

Yuanyuan Duan and Yili Hong
Department of Statistics
Virginia Tech
Blacksburg, VA 24061
E-mail: yyduan@vt.edu
yilihong@vt.edu

William Q. Meeker
Department of Statistics
Iowa State University
Ames, IA 50011
E-mail: wqmeeker@iastate.edu

Deborah L. Stanley and Xiaohong Gu
Engineering Laboratory
National Institute of Standards & Technology
Gaithersburg, MD 20899
E-mail: debbie.stanley@nist.gov
xiaohong.gu@nist.gov